Identifying Kinetic Model Parameters and Implementing 3-DOF Control for a Dual-Thruster USV: A Case Study Using the VRX Simulation Environment

Jungeun Yoon[a] and Rockwon Kim[b]
ETRI, South Korea
{*yje3058, rwkim*}*@etri.re.kr*

Keywords: Unmanned Surface Vehicle, Dual Thrust, 3-DOF Model, Parameter Identification, Gazebo Simulation.

Abstract: This study addresses the challenge of creating accurate kinetic model-based simulations for Unmanned Surface Vehicles (USVs) that replicate the VRX simulation environment. Without precise parameter estimation, discrepancies arise between kinetic model-based position predictions and the USV's position in the VRX simulation. We propose a comprehensive method for parameter estimation to bridge this gap, coupled with a Dynamical PD+LOS controller to further minimize operational differences. In the control using the kinetic model with the best fit thrust parameters and drag coefficients, the turning radius may vary depending on these parameters. To handle this, it not only calculates the thrust difference based on the heading error but also dynamically adjusts the base thrust according to the speed and distance to the target. This approach prevents over-correction and ensures better alignment between the kinetic model prediction path and VRX movement. The proposed methodology was validated through circle and zigzag path tests. Results demonstrated high fidelity, with position errors of 2% and time errors of 0.37% between the VRX and kinetic model.

1 INTRODUCTION

Unmanned surface vehicles (USVs) have recently gained significant attention due to their diverse applications in marine engineering. To effectively operate USV systems, it is crucial to accurately understand each vessel's kinetic and dynamic characteristics. Specifically, quantitatively analyzing and controlling USVs requires precise identification of their dynamic equations and physical parameters. However, when adding autonomous navigation capabilities to remotely controlled small boats designed for rivers, lakes, and coastal areas, we often encounter situations where the kinetic model parameters are unknown. In such scenarios, parameter estimation and the subsequent use of kinetic model-based path generation simulations become critical prerequisites for USV control.

Traditionally, parameter estimation has heavily relied on methods such as the Kalman filter (Yoon and Rhee, 2003) and recursive least squaress (Nguyen, 2008). More recently, modern artificial intelligence techniques have been employed to identify the dynamic models of ships (Wang et al., 2019; Woo et al., 2018). Wirtensohn et al. conducted a quality evaluation of parameter identification for small USVs and performed sensitivity analysis using the Fisher information matrix. During the identification process, all parameters were estimated simultaneously, and a correlation matrix was used to analyze interdependencies among parameters. Eigenvalue and eigenvector analyses were also performed to avoid overparameterization (Wirtensohn et al., 2015). Xu et al. proposed a method for identifying the dynamic model of USVs that discretizes the Abkowitz model and utilizes a Cuckoo Search (CS) algorithm-enhanced Support Vector Machine (SVM) method. This approach achieves more accurate identification of the 3-degree-of-freedom (3-DOF) dynamic model of USVs and was validated through experimental tests and data analysis conducted on the Qinghuai River (Xu et al., 2020).

In this study, we propose a method for parameter estimation and control using the OpenRobotics' Virtual RobotX (VRX) simulation environment instead of a physical USV. VRX offers extensive capabilities for research in USV control system design. VRX enables the attachment and data collection from diverse sensors such as GPS, IMU, LiDAR, and cameras on

[a] https://orcid.org/0009-0006-3461-0693
[b] https://orcid.org/0009-0007-7329-9401

Yoon, J. and Kim, R.
Identifying Kinetic Model Parameters and Implementing 3-DOF Control for a Dual-Thruster USV: A Case Study Using the VRX Simulation Environment.
DOI: 10.5220/0013010600003822

In *Proceedings of the 21st International Conference on Informatics in Control, Automation and Robotics (ICINCO 2024) - Volume 1*, pages 368-375
ISBN: 978-989-758-717-7; ISSN: 2184-2809

ships, and as a ROS environment simulator, it facilitates the easy addition or removal of USV sensors and motors (Bayrak and Bayram, 2023; Li et al., 2023; Wu and Wei, 2023; Chu et al., 2024). This allows for replicating the thruster configuration of real USVs in a virtual environment, enabling the modeling of various USV motions. VRX simulation offers advantages in terms of cost and time compared to real experiments, allowing for efficient and safe testing under various environment conditions (Huang et al., 2023; Bingham et al., 2019; Paravisi et al., 2019).

The 3-DOF kinetic model can predict and generate paths quickly by setting the time interval as a variable and using iterative loops. The generated paths vary depending on kinetic model parameters, such as drag coefficients, inertia, and thrust. Based on previous studies (Li et al., 2019), we estimated the USV parameters in the VRX simulator. However, the kinetic model failed to generate the correct path to reach the target in the VRX simulation. The reason is that incorrect thrust parameters and drag coefficients were identified, which resulted from incorrectly determining the point at which the USV reaches a steady state in the VRX simulation. This issue will be discussed in detail in Section 2.3. Therefore, this study refines the parameter estimation methods from previous research to improve accuracy in VRX simulations. When applying the correctly identified parameters to the kinetic model to generate paths, an issue arose where the turning radius became larger. To resolve this, we propose a control algorithm that enables the USV to reach the target point more quickly with a smaller turning radius. To address these issues, our study focuses on the following:

- First, unlike previous studies, we aim to simultaneously identify the propulsion force parameters and surge-direction drag coefficients by applying an iterative optimization method. To achieve this, we use velocity variation data from multiple linear motion tests under different thrust conditions. (While the propulsion parameters are unknown, we can control certain conditions, such as revolutions per second.)
- Second, We propose a new thrust control algorithm for USVs. This algorithm addresses the challenge of controlling USVs with large turning radius, which can lead to inefficient navigation. Our approach considers not only heading error but also velocity and distance to the target. This comprehensive control strategy enables more efficient path planning and optimized navigation, especially in situations where the turning radius increases. Furthermore, this thrust control approach contributes to minimizing the gap between the trajectory and timing predicted by the kinetic model and the behavior of the USV controlled by the kinetic model within the VRX simulator.

The structure of this paper is as follows: Section 2.1 provides a brief introduction to the VRX simulation environment and the specifications of the USV. Section 2.2 describes the dynamics of the USV. Section 2.3 proposes a parameter identification procedure for the dual thruster model using the Nelder-Mead algorithm. Section 2.4 identifies the drag matrix parameters through VRX simulation driving tests and performs corrections to enhance the accuracy of the kinetic model. Section 2.5 proposes a USV control system applying the improved PD controller and validates it through circle and zigzag simulations. Finally, Section 3 summarizes the conclusions.

2 METHODOLOGY

2.1 Simulation Environment

In this study, we identify the kinetic model parameters using the VRX ROS2 package from Open Robotics and the Gazebo simulator environment. The USV model supported by VRX is the WAM-V (Bingham et al., 2019), with its specifications listed in Table 1. Experiments were conducted in the Sydney Regatta world, one of the various environments provided by VRX. To eliminate the effects of external forces, both wind and wave parameters were set to zero. Additionally, to focus on the validity of the parameter extraction method, GPS and IMU sensor errors were also set to zero.

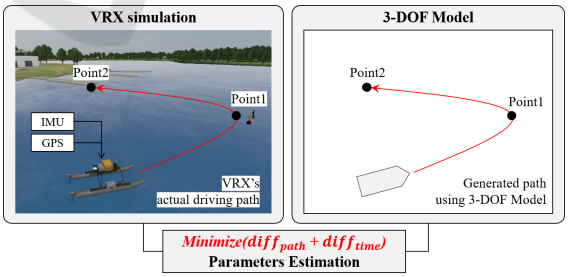

Figure 1: Parameter estimation to minimize and control discrepancies between VRX and Kinetic Model trajectories.

2.2 3-DOF Kinetic Model for Dual Thruster USV

The 3-DOF mathematical model of USV is used to mathematically represent the position and physical motion of the vehicle, reflecting the characteristics of

Table 1: Physical characteristics of the WAM-V USV.

Parameter	Value
Length overall (LO)	4.00 m
Waterline length (L)	3.21 m
Draft (D)	0.089 m
Beam overall (W)	2.44 m
Distance between two propellers (B)	2.01 m
Mass (m)	180 kg
USV velocity (max)	1.5 m/s

the USV and optimizing its driving control. As explained in (Fossen, 2011), the 3-DOF mathematical model of USV can be described as follows:

$$\dot{\eta} = \begin{bmatrix} \dot{x} \\ \dot{y} \\ \dot{\psi} \end{bmatrix} = R(\psi)\mathbf{v} = \begin{bmatrix} \cos\psi & -\sin\psi & 0 \\ \sin\psi & \cos\psi & 0 \\ 0 & 0 & 1 \end{bmatrix} \begin{bmatrix} u \\ v \\ r \end{bmatrix} \tag{1}$$

$$M\dot{\mathbf{v}} + C(\mathbf{v})\mathbf{v} + D(\mathbf{v})\mathbf{v} = \tau \tag{2}$$

$\eta = \begin{bmatrix} x\ y\ \psi \end{bmatrix}$, where $\eta_t = \eta_{t-1} + \dot{\eta}\Delta t$, is a vector that defines the position and orientation of the USV. Here, x and y are the position coordinates in the plane, ψ is the heading angle, η_t and η_{t-1} represent the current and previous states respectively, $\dot{\eta}_t$ is the rate of change, and Δt is the time interval between states. $\mathbf{v} = \begin{bmatrix} u\ v\ r \end{bmatrix}$ is a vector consisting of the linear velocities (u, v) in the surge and sway directions and the rotational velocity (r). $R(\psi)$ is a rotation matrix that transforms from the fixed body frame to the earth-fixed frame.

In Equation (2), $\mathbf{M}$, $\mathbf{C}(\mathbf{v})$, and $\mathbf{D}(\mathbf{v})$ represent the mass matrix, the Coriolis and centripetal matrix, and the drag matrix, respectively. τ is a vector representing the force generated by the thruster, where T_1 is the force of the port thruster and T_2 is the force of the starboard thruster.

The matrix M accounts for both the rigid-body mass and the hydrodynamic added mass effects in surge, sway, and yaw motions. For notational convenience, $m - X_{\dot{u}}$, $m - Y_{\dot{v}}$, and $I_z - N_{\dot{r}}$ are denoted as m_{11}, m_{22}, and m_{33} respectively, where m_{11} and m_{22} represent the total mass (including added mass) in the surge and sway directions respectively, and m_{33} represents the total moment of inertia (including added moment) about the z-axis.

The following describes the vectors and matrices of the kinetic model, which can be simplified under the following conditions (Li et al., 2019):

- Low USV velocity: In this study, the maximum velocity is 1.5 m/s.
- Negligible Effect of Off-Diagonal Terms on USV Dynamics: The off-diagonal terms of M and D can be neglected.
- Assuming the USV sails in a calm environment.

$$\mathbf{M} = \begin{bmatrix} m_{11} & 0 & 0 \\ 0 & m_{22} & 0 \\ 0 & 0 & m_{33} \end{bmatrix} \tag{3}$$

$$\mathbf{C}(\mathbf{v}) = \begin{bmatrix} 0 & 0 & -m_{22}v \\ 0 & 0 & m_{11}u \\ m_{22}v & -m_{11}u & 0 \end{bmatrix} \tag{4}$$

$$\mathbf{D}(\mathbf{v}) = \mathbf{D} = -\begin{bmatrix} X_u & 0 & 0 \\ 0 & Y_v & 0 \\ 0 & 0 & N_r \end{bmatrix} \tag{5}$$

$$\tau = \begin{bmatrix} T_1 + T_2 & 0 & (T_1 - T_2) \cdot d_P \end{bmatrix}^T \tag{6}$$

Therefore, the 3-DOF model of a USV with dual thrusters without a rudder can be expressed as Equation (7), in which d_p represents half the distance between the two propellers. This model enables us to iteratively generate a movement path by calculating the necessary corrective thrust at each subsequent position, accounting for positional errors and continuously adjusting the control inputs. In actual VRX movement, GPS and IMU yaw data are utilized for navigation. To reduce the difference between these two, we must estimate the parameters of the thrust equation and the drag coefficients X_u, Y_v, and N_u with a certain degree of precision.

$$\begin{aligned} m_{11}\dot{u} - m_{22}\dot{v}r + X_u u &= T_1 + T_2 \\ m_{22}\dot{v} + m_{11}ur + Y_v v &= 0 \\ m_{33}\dot{r} - (m_{11} - m_{22})uv + N_r r &= (T_1 - T_2) \cdot d_P \end{aligned} \tag{7}$$

2.3 Identification of Thrust Coefficients

The thrust of a dual-thruster USV is determined by both the propeller and the hull velocity is described by Equation (8)(Mu et al., 2018). In this equation, n represents the propeller's rotational speed in revolutions per second (RPS), and $V = \sqrt{u^2 + v^2}$ denotes the total velocity of the USV. c and d are the key parameters of the thrust model. The coefficient c reflects the interaction between the hull velocity and propeller rotation, while d represents the thrust generation characteristics of the propeller itself.

$$T_i = cVn_i + d|n_i|n_i \tag{8}$$

To achieve accurate velocity and position estimation, it is essential to determine the coefficients c and d that closely approximate the actual thrust. To

achieve this, we can approximate the coefficients c and d by utilizing the straight-line motion equation from the kinetic model, which allows us to reduce the number of variables. In a straight-line motion, the Coriolis force is canceled as $v = r = 0$, and the velocity only has a surge component. Consequently, the model can be simplified to a 1-DOF model, only including surge velocity, as follows:

Li et al. collected velocity, acceleration, and RPS data for a stationary USV to estimate the coefficients c and d (Li et al., 2019). However, as shown in Fig. 2, the data collected from the VRX sensor exhibited significant instability and fluctuations. This instability made it ambiguous to determine a reliable point for calculating initial acceleration when estimating the c and d values for the VRX thrust equation using Li's method. Consequently, to minimize potential errors, we propose estimating the c and d values without considering the acceleration value.

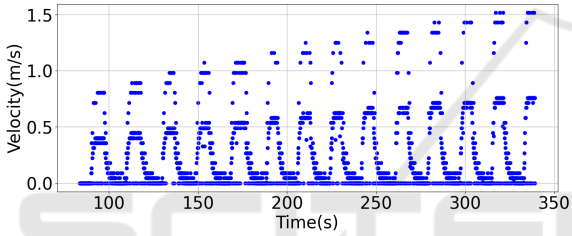

Figure 2: Visualization of velocity data collected using VRX.

When the USV maintains a constant surge velocity, the surge acceleration becomes zero. Consequently, the thrust model can be simplified, as shown in Equation (9). Using the Nelder-Mead algorithm, we estimate the values of c, d, and X_u in this simplified model. This is especially important because the velocity data exhibits high nonlinearity, irregular variability, and clear discontinuities, suggesting a complex, non-differentiable objective function. The Nelder-Mead algorithm is well-suited to handle such nonlinear optimization problems effectively without requiring derivatives, thanks to its robustness to noise and ability to manage discontinuities. Additionally, the simplicity and computational efficiency of the algorithm make it advantageous in this situation, where a large number of data points must be processed.

$$X_u u = 2(cun + d|n|n), n = n_1 = n_2 \quad (9)$$

Data for estimating the values of c, d, and X_u are collected through straight-line motion experiments. The procedure is as follows: First, the USV is brought to a complete stop to stabilize its state before each run. Then, the thrust value is adjusted. Once the USV reaches the point where the speed oscillates with the same amplitude between increasing and decreasing, velocity and propeller RPS data are collected.

Based on the collected data, we can estimate the values as $c = -0.397956$, $d = 0.299914$, and $X_u = 145.75$. Substituting these values into Equation (9), we can calculate the thrust value of the USV as shown in Equation (10).

$$T_i = -0.397956\sqrt{u^2+v^2}\cdot n_i + 0.299914|n_i|\cdot n_i \quad (10)$$

As shown in Fig 3, repeated experiments on the relationship between thrust and velocity in the VRX simulator revealed that the USV reached a maximum speed of 1.5 m/s at the highest thrust value of 250. It was observed that the USV would not move when the thrust was below 30 due to resistance. Considering these characteristics, the effective thrust range for the simulation was set between 30 and 250.

The blue curve in the Fig 3 is the estimated thrust curve fitted based on Equation (10) with a maximum surge velocity of $1.5m/s$ and sway velocity of $0m/s$. The red dots represent the RPS values observed in VRX by inputting thrust values to the port and starboard thrusters, with the USV velocity at that time indicated by arrows. The fact that the two sets of values coincide suggests that the thrust parameters c and d have been correctly estimated.

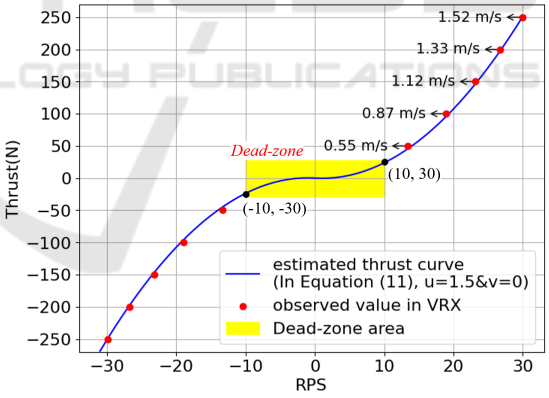

Figure 3: The relationship between RPS and thrust.

2.4 Identification of Drag Coefficients

To identify N_r and Y_v, experiments were conducted with zero-radius rotation ($r \approx 0$) and non-zero radius turning ($r > 0$) respectively, by configuring different RPS values for the port and starboard thrusters of the USV. Velocity vector v data was collected from these experiments and then used to estimate the parameters using the Nelder-Mead algorithm.

To achieve zero-radius rotation, the USV's port and starboard thruster revolutions per second (RPS)

were set to -30 and 30 respectively for 30 seconds. This configuration caused the USV to rotate around its center of gravity while minimizing surge and sway velocities. Under these conditions, where $\dot{r} \approx u \approx v \approx 0$, the rotation drag coefficient N_r could be estimated using Equation (11).

$$N_r r = (T_1 - T_2) \cdot d_P \tag{11}$$

Similarly, for the sway direction drag coefficient Y_v, by running the thrusters with an RPS of 0 and 30 for 60 seconds, the USV travels with a larger non-zero radius turning maneuver. Y_v can be estimated based on Equation (12).

$$m_{22}\dot{v} + m_{11}ur + Y_v v = 0 \tag{12}$$

The mass matrix M can be calculated as follows according to the USV specifications in Table 1 (Muske et al., 2008).

$$m_{11} \approx m + 0.05m = 189 \tag{13}$$

$$m_{22} \approx m + 0.5(\rho\pi D^2 L) = 229 \tag{14}$$

$$m_{33} \approx \frac{m(L^2 + W^2) + \frac{1}{2}(0.1mB^2 + \rho\pi D^2 L^3)}{12} = 333 \tag{15}$$

Therefore, the drag coefficients were estimated as $X_u = 145$, $Y_v = 56$, and $N_r = 1023$. When these drag parameter values were applied to the kinetic model, a problem arose where the surge velocity calculated by the kinetic model was faster than the VRX simulation, as shown in Fig. 4a. This resulted in a mismatch between the VRX and kinetic model. This discrepancy suggests that there is an error in the kinetic model parameters.

The method presented in Section 2.3 requires reaching a state of constant acceleration, but the difficulty in clearly distinguishing the point of constant acceleration led to an incorrect identification. To address this, the acceleration calculated from the experimental data set used to estimate c and d is compared to the acceleration calculated from Equation (16), and the error is used to re-adjust the X_u value for correction. Similarly, N_r can also be corrected using the same approach.

$$\dot{u} = \frac{(T_1 + T_2) + m_{22}vr - X_u u}{m_{11}} \tag{16}$$

$$\dot{r} = \frac{(T_1 - T_2)d_p + (m_{11} - m_{22})uv - N_r r}{m_{33}} \tag{17}$$

Since the drag parameters do not have a significant impact at low velocities, data corresponding to more

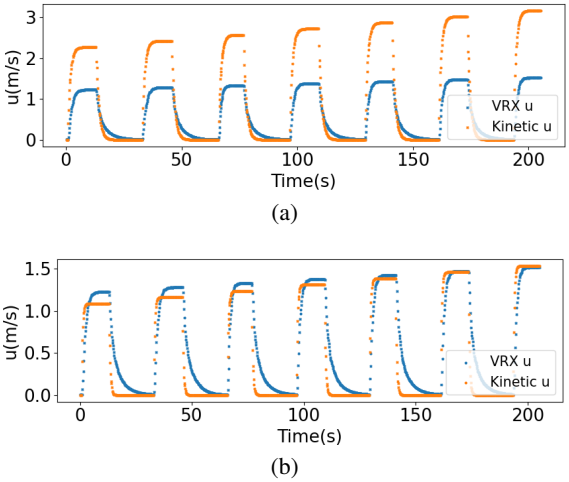

Figure 4: VRX-collected and kinetic model-calculated velocity: (a) Before correction and (b) After correction.

than 70% of the maximum velocity was collected and used for the correction. As a result, the values of X_u and N_r were re-identified as $X_u = 340$ and $N_r = 1012$, and as shown in Fig 4b, the velocity was improved compared to Fig 4a when applied to the kinetic model.

2.5 USV Motion Control System

In USV motion control systems, the design of path-following controllers plays a crucial role in enabling real-world navigation. Proportional-Derivative (PD) control is widely used in autonomous navigation due to its simple structure and high stability, while the Line of Sight(LOS) algorithm offers the advantages of low computational complexity and ease of implementation (Mu et al., 2017; Sarda et al., 2015). In this study, we utilized a USV control system that combines PD control and the LOS algorithm. As shown in the Fig 5, the LOS algorithm calculates the error between the current position and the target position, and PD control determines the thrust of the port and starboard thrusters based on the error.

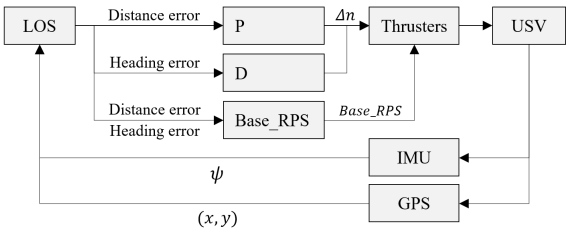

Figure 5: The USV motion control system.

The LOS algorithm guides the USV to navigate along the line connecting the target points on the tracking path. As the USV approaches the desired

path, the distance gradually decreases, allowing it to follow the desired path (Lekkas and Fossen, 2012). In Fig 6, (x,y) represents the coordinates of the current position, and ψ represents the heading value of the USV at the current position. (x_t,y_t) represents the coordinates of the target position, and ψ_d represents the target heading value for reaching the target point. In this case, ψ_d can be calculated as $\arctan\left(\frac{\Delta y}{\Delta x}\right)$, as shown in Fig 6. The heading error between the current position and the target position can be obtained as $\psi_e = \psi - \psi_d$.

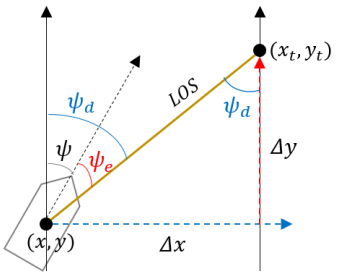

Figure 6: The principle of the LOS guidance algorithm.

The *Base_RPS* in the Fig 5 represents the base value for the RPS. It is dynamically adjusted based on the distance error, which is the distance between the current and target positions, and the value of e_t according to the algorithm 1. When the distance is less than dis_{min} and the e_t is small, indicating proximity to the target position, the base value is set to the minimum value. When the distance is less than dis_{min} but the e_t is large, a constant velocity must be maintained to enable rotation. therefore, the midpoint between dis_{min} and dis_{max} becomes the base value. If the distance falls between dis_{min} and dis_{max}, linear interpolation is used to determine the base value based on the distance ratio. In other cases, when the distance is large, the maximum velocity is set as the base value.

The output of the PD controller is Δn, which is the difference in rotation velocity between the port and starboard thrusters, thrust values of the port and starboard thrusters are set combine *basen* and Δn.The derivative part is sensitive to noise, and a first-order low-pass filter is added, as expressed in Equation (18). Here, T_f is the time constant of the filter, and df_{t-1} is the differential output value of the previous moment. T is the period of the PD controller.

Conventional PD controllers utilize fixed constant values for their gain parameters, K_p and K_d. The gains K_p and K_d of the PD controller were experimentally tuned through kinetic model, with values gradually adjusted from small to large until the USV could accurately follow the target points. This approach has

Procedure *GetDynamicBaseN(*
$\psi_{e_t}, dis_t, dis_{min}, dis_{max}, base_{min}, base_{max}$*)*:
  $n \leftarrow 0$;
  if $dis_t < dis_{min} \wedge \psi_{e_t} < 10°$ **then**
    $n \leftarrow base_{min}$;
  else
    if $dis_t < dis_{min} \wedge \psi_{e_t} \geq 10°$ **then**
      $n \leftarrow base_{min} + (base_{max} - base_{min}) \times 0.5$;
    else
      if $dis_t \geq dis_{min} \wedge dis_t \leq dis_{max}$ **then**
        $n \leftarrow base_{min} + (base_{max} - base_{min}) \times (dis_t - dis_{min})/(dis_{max} - dis_{min})$;
      else
        $n \leftarrow base_{max}$;
      end
    end
  end
  return n;

Algorithm 1: Dynamic Base RPS Calculation.

the drawback of an increased turning radius, as shown by the orange dotted line in Fig 7. To reach the target point more quickly with a smaller turning radius, we dynamically adjusted the gain value based on the current position using Equation (18). Consequently, it is able to reduce the turning radius, as shown by the blue line.

K_p is a proportional control variable that reflects the distance between two points, providing a larger control signal as the distance increases. K_d is a differential control variable that reflects the ψ_e value, designed to respond more sensitively as the error rate increases. To prevent the values of each control variable from changing abruptly, the log function is applied.

$$\Delta n = K_p \cdot \log(dis_t) \cdot \psi_{e_t} + \left(\frac{T_f}{T_f + T}\right) \cdot df_{t-1} + \left(\frac{K_d \cdot \log(\psi_e)}{T_f + T}\right) \cdot (\psi_{e_t} - \psi_{e_{t-1}}) \quad (18)$$

The USV motion control system calculates the thrust values of the port and starboard thrusters by considering both distance error and heading error, enabling precise navigation.

The circle and zigzag driving tests were conducted to estimate kinetic model parameters and validate control algorithms. The kinetic model and VRX simulation were set up under the same conditions. Fig 8 shows the experimental results for tests. While each path does not perfectly match, it can be confirmed that the vehicle follows a similar path. The time error for the circle test was about 2%, and there was no error in the zigzag test. The distance error showed low errors of about 0.37% for both circle and zigzag tests.

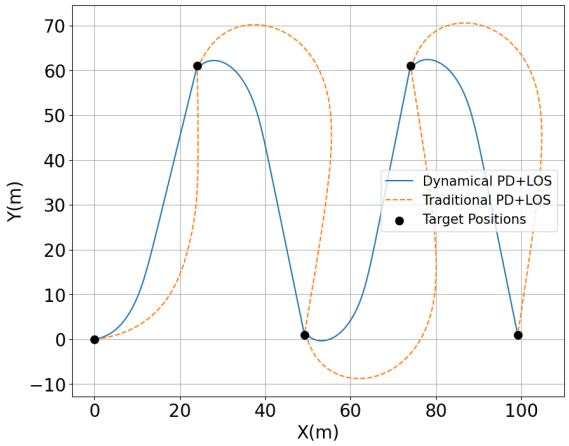

Figure 7: The simulation results of the kinetic-model.

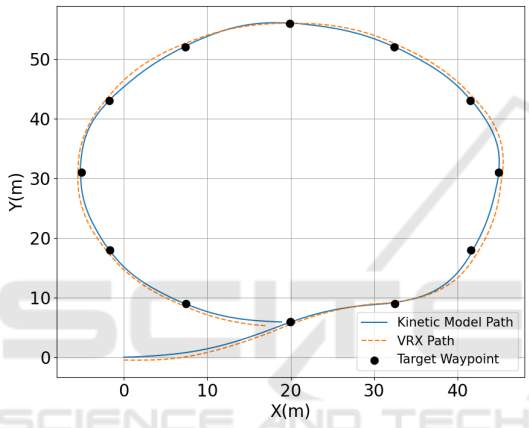

(a)

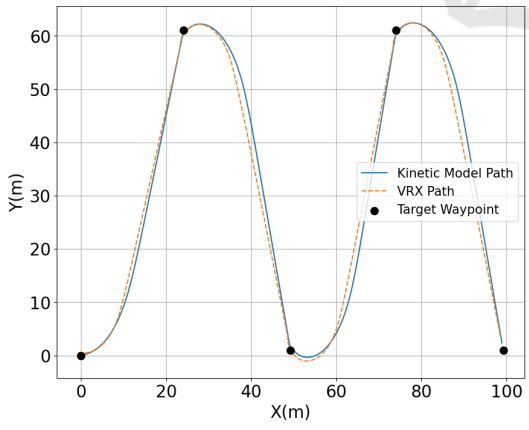

(b)

Figure 8: The simulation results of the kinetic-model and VRX path: (a) circle path and (b) zigzag path.

3 CONCLUSION

This paper addressed the development of a control method using a 3-DOF kinetic model in the VRX simulation environment, as well as the accurate identification of the necessary parameters for this model.

We proposed a method for determining propulsion force parameters and drag coefficients using the Nelder-Mead algorithm.

This method simultaneously estimates the values of propulsion force parameters and surge-direction drag coefficients using a simplified surge motion equation, based on linear motion velocity data obtained under various thrust speeds.

Additionally, we developed a dynamical PD+LOS control algorithm that minimizes position and time discrepancies between movement in VRX and the kinetic model prediction path. This algorithm does not provide a fixed differential thrust for heading errors; instead, it offers varying differential thrust even for the same heading error by considering the current velocity and distance to the target point. This method enables the generation of optimized paths, effectively adapting to changes in velocity and turning radius in response to thrust, which may vary based on the identified parameters. The validity of the proposed methodology was verified through circle and zigzag path tests. Results demonstrated high fidelity, with position errors of 2% and time errors of 0.37% between the movement in the VRX simulation and the kinetic model-generated path.

This study contributes to enhancing the learning value of the open-source VRX simulator for understanding 3-DOF control of small USVs' kinetic models. While VRX is a well-designed simulator that offers a cost-effective alternative to real-world experiments, its utility for educational purposes was limited by discrepancies between simulated and theoretical behaviors. Our work addresses these inconsistencies, potentially improving VRX's effectiveness as a learning tool for small USV dynamics and control. By refining the parameter estimation and control algorithms, we aim to bridge the gap between simulation and theoretical models, thus supporting more accurate and reliable learning experiences in USV control systems.

Future research could focus on testing the model's performance under various maritime environmental conditions and extending the methodology to more complex path and mission scenarios. Additionally, validation experiments in real marine environments could further strengthen the practicality of the proposed method.

ACKNOWLEDGEMENTS

This work was supported by SME ICT convergence technologies project in Andong-si [24AD1100]. This work was supported by Electronics and Telecommunications Research Institute(ETRI) grant funded by the Korean government. [24ZD1110, Regional Industry ICT Convergence Technology Advancement and Support Project in Daegu-Gyeongbuk].

REFERENCES

Bayrak, M. and Bayram, H. (2023). Colreg-compliant simulation environment for verifying usv motion planning algorithms. In *OCEANS 2023-Limerick*, pages 1–10. IEEE.

Bingham, B., Aguero, C., McCarrin, M., Klamo, J., Malia, J., Allen, K., Lum, T., Rawson, M., and Waqar, R. (2019). Toward maritime robotic simulation in gazebo. In *Proceedings of MTS/IEEE OCEANS Conference*, Seattle, WA.

Chu, Y., Wu, Z., Zhu, X., Yue, Y., Lim, E. G., and Paoletti, P. (2024). Self-supervised dock pose estimator for unmanned surface vehicles autonomous docking. In *2024 10th International Conference on Mechatronics and Robotics Engineering (ICMRE)*, pages 189–194. IEEE.

Fossen, T. I. (2011). *Handbook of marine craft hydrodynamics and motion control*. John Wiley & Sons.

Huang, F., Chen, X., Xu, Y., Yang, X., and Chen, Z. (2023). Immersive virtual simulation system design for the guidance, navigation and control of unmanned surface vehicles. *Ocean Engineering*, 281:114884.

Lekkas, A. M. and Fossen, T. I. (2012). A time-varying lookahead distance guidance law for path following. *IFAC Proceedings Volumes*, 45(27):398–403. 9th IFAC Conference on Manoeuvring and Control of Marine Craft.

Li, C., Jiang, J., Duan, F., Liu, W., Wang, X., Bu, L., Sun, Z., and Yang, G. (2019). Modeling and experimental testing of an unmanned surface vehicle with rudderless double thrusters. *Sensors*, 19(9).

Li, J., Chavez-Galaviz, J., Azizzadenesheli, K., and Mahmoudian, N. (2023). Dynamic obstacle avoidance for usvs using cross-domain deep reinforcement learning and neural network model predictive controller. *Sensors*, 23(7):3572.

Mu, D., Wang, G., Fan, Y., Sun, X., and Qiu, B. (2017). Adaptive los path following for a podded propulsion unmanned surface vehicle with uncertainty of model and actuator saturation. *Applied Sciences*, 7(12).

Mu, D., Wang, G., Fan, Y., Sun, X., and Qiu, B. (2018). Modeling and identification for vector propulsion of an unmanned surface vehicle: Three degrees of freedom model and response model. *Sensors*, 18(6).

Muske, K. R., Ashrafiuon, H., Haas, G., McCloskey, R., and Flynn, T. (2008). Identification of a control oriented nonlinear dynamic usv model. In *2008 American Control Conference*, pages 562–567.

Nguyen, H. D. (2008). Recursive identification of ship manoeuvring dynamics and hydrodynamics. In Mercer, G. N. and Roberts, A. J., editors, *Proceedings of the 8th Biennial Engineering Mathematics and Applications Conference, EMAC-2007*, volume 49 of *ANZIAM J.*, pages C717–C732.

Paravisi, M., H. Santos, D., Jorge, V., Heck, G., Gonçalves, L. M., and Amory, A. (2019). Unmanned surface vehicle simulator with realistic environmental disturbances. *Sensors*, 19(5).

Sarda, E. I., Bertaska, I. R., Qu, A., and von Ellenrieder, K. D. (2015). Development of a usv station-keeping controller. In *OCEANS 2015-Genova*, pages 1–10. IEEE.

Wang, Z., Zou, Z., and Guedes Soares, C. (2019). Identification of ship manoeuvring motion based on nu-support vector machine. *Ocean Engineering*, 183:270–281.

Wirtensohn, S., Wenzl, H., Tietz, T., and Reuter, J. (2015). Parameter identification and validation analysis for a small usv. In *2015 20th International Conference on Methods and Models in Automation and Robotics (MMAR)*, pages 701–706.

Woo, J., Park, J., Yu, C., and Kim, N. (2018). Dynamic model identification of unmanned surface vehicles using deep learning network. *Applied Ocean Research*, 78:123–133.

Wu, X. and Wei, C. (2023). Drl-based motion control for unmanned surface vehicles with environmental disturbances. In *2023 IEEE International Conference on Unmanned Systems (ICUS)*, pages 1696–1700. IEEE.

Xu, P.-F., Cheng, C., Cheng, H.-X., Shen, Y.-L., and Ding, Y.-X. (2020). Identification-based 3 dof model of unmanned surface vehicle using support vector machines enhanced by cuckoo search algorithm. *Ocean Engineering*, 197:106898.

Yoon, H. K. and Rhee, K. P. (2003). Identification of hydrodynamic coefficients in ship maneuvering equations of motion by estimation-before-modeling technique. *Ocean Engineering*, 30(18):2379–2404.